Available online at www.sciencedirect.com
SCIENCE DIRECT®
Journal of Nuclear Materials 349 (2006) 317–326
journal of nuclear materials
www.elsevier.com/locate/jnucmat

Thermodynamics of Fe–Cu alloys as described by a classic potential

A. Caro [a,*], M. Caro [b], E.M. Lopasso [b], P.E.A. Turchi [a], D. Farkas [c]

[a] *Lawrence Livermore National Laboratory, P.O. Box 808, Livermore, CA 94551, USA*
[b] *Centro Atómico Bariloche, 8400 Bariloche, Argentina*
[c] *Department of Materials Science and Engineering, Virginia Tech., Blacksburg, VA 24061, USA*

Received 19 April 2005; accepted 1 November 2005

Abstract

The Fe–Cu system is of relevance to the nuclear industry because of the deleterious consequences of Cu precipitates in the mechanical properties of Fe. Several sets of classical potentials are used in molecular dynamics simulations studies of this system, in particular that proposed by Ludwig et al. [M. Ludwig, D. Farkas, D. Pedraza, S. Schmauder, Model. Simul. Mater. Sci. Eng. 6 (1998) 19]. In this work we extract thermodynamic information from this interatomic potential. We obtain equilibrium phase diagram and find a reasonable agreement with the experimental phases in the regions of relevance to radiation damage studies. We compare the results with the predicted phase diagram based on other potential, as calculated in previous work. We discuss the disagreements found between the phase diagram calculated here and experimental results, focusing on the pure components and discuss the applicability of these potentials. Improved potentials, primarily for the pure components, should be developed to account for proper phase stability in the solid phase up to melting. Finally we suggest an approach to improve existing potentials for this system.

PACS: 81.30.Bx; 82.60.Lf; 02.70.Ns; 65.40.−b; 64.75.+g; 82.20.Wt

1. Introduction

As Computational Materials Science becomes a standard approach to study complex problems in solids, the requirement of accurate, predictive simulation tools stresses the necessity of models for the interactions that are able to reproduce important fundamental properties of materials. To capture the length scale that is relevant to study mechanical properties and microstructures, simple classical empirical total energy expressions are required to deal with the large number of atoms this class of problems requires. Usually the models used are of the Embedded Atom Method (EAM) type, referred to as 'many-body' potentials. Most of the vast amount of work done using these classical potentials addresses either pure elements or intermetallic compounds, only a few address alloys.

Many properties of some pure materials, in particular the late fcc transition metals, are well reproduced

* Corresponding author.
E-mail address: caro2@llnl.gov (A. Caro).

0022-3115/$ - see front matter © 2005 Elsevier B.V. All rights reserved.
doi:10.1016/j.jnucmat.2005.11.004

with this approach. For other metals, and in particular Fe, the situation is much less satisfactory, due to the importance of magnetism and the angular components of bonding in this material. In addition, most of the available potentials for the pure components are only tested at low temperature.

Computational materials science has being paying attention to Fe–Cu for a long time, to follow the radiation-induced Cu precipitation. The first report on bcc Cu precipitates dates from 1990 [1,2] using a potential that has a stable bcc phase for Cu [3], but this study did not address the Fe–Cu problem because of the absence of an alloy potential. The first potential for the alloy appeared in 1995 [4–6] and precipitation as well as vacancy formation inside the precipitates were studied. Using a simplified energetics, lattice Monte Carlo simulations were extensively used to analyze precipitation [7–9]. A different Fe–Cu potential was proposed in 1998 [10] and used to study the coherency loss of precipitates [11]. Additional coherence loss studies were reported in 2001 [12] using a potential reported in [3].

In a recent series of papers, we addressed the problem of alloy description from the perspective of thermodynamics rather than from the properties of a single impurity. We developed a series of codes that calculate the free energy of a given phase by implementing the switching Hamiltonian technique. We applied the methodology to Au–Ni alloys based on a single lattice (fcc) with a miscibility gap [13,14], and to the more complex Fe–Cu system as described by the Ackland–Bacon potential [15]. That work showed various shortcomings of these potentials with significant differences with the experimental phase diagram [16]. In the present work, we analyze the thermodynamics of Fe–Cu as predicted by the Ludwig–Farkas potential [10], built upon the Cu potential given by Voter [17] and the Fe potential given by Simonelli et al. [18]. The goal is to test the validity of this description for radiation damage studies and to present a comparative study that will help guide future development of interatomic potentials for alloys in this system. In the following section, we give a summary of the computational method, with references to the full description that we already published. In Section 3 we present the calculated phase diagram and discuss the thermodynamic properties of the unaries Cu and Fe and of the Fe–Cu alloy system. We show that these potentials give a better agreement in the regions of the phase diagram relevant to radiation damage studies. We then discuss the regions where agreement needs to be improved. We show that most of the shortcomings are in the regions of the pure components and point out the properties that need to be improved in order to obtain a better description of this alloys system.

2. Free energy determination

The calculation of the thermodynamic properties of an alloy implies the knowledge of the free energy of the different phases as a function of composition and temperature. The calculation of the free energy is a multi-step process that requires several different molecular dynamics (MD) runs. In recent papers, we implemented a numerical package that allows efficient and accurate calculation of it. For a complete description of the method, we refer the reader to those previous publications [13–15]. Here we only highlight its basic aspects, together with the main equations.

Following the methodology proposed in CALPHAD [19,20] we separate the problem of binary alloys in terms of the properties of the pure elements (i.e., the free energies of all possible phases of the pure elements) and the properties of the mixtures. The later are expressed in terms of excess enthalpy, entropy and free energy. Excess quantities are referred to the linear interpolation between the pure elements, which represents the ideal solution. In this way, the alloy description is conveniently separated in two distinct parts: the description of the pure elements on one hand, and the description of the mixture on the other. The CALPHAD approach is a standardized way to express the thermodynamic information of a system. Once the free energies are expressed in this way (suggested by the Scientific Group Thermodata Europe (SGTE) [21]), the calculation of the quantities of interest and phase diagrams can easily be performed with available application software such as Thermo-Calc [22]. Our numerical results can be compared with those from thermodynamic databases that contain the most accepted values for these quantities, taken from Dinsdale's compilation [23]. The latter constitute for us what we take as experimental values although not all data in the database are from experimental assessment.

Let us first describe the procedure for the pure element case. Using the Gibbs–Duhem equation we calculate the free energy per particle at a given temperature T, $f(T)$. This equation is a thermody-

namic integration between the state of interest and a reference state at temperature T_0 with known free energy $f(T_0)$,

$$f(T) = f(T_0)\frac{T}{T_0} - T\int_{T_0}^{T}\frac{h(\tau)}{\tau^2}\,\mathrm{d}\tau, \tag{1}$$

where $h(\tau)$ is the enthalpy per particle. The enthalpy is easily obtained from a MD run, and it is fitted with a second-order polynomial in T that allows an analytic integration in Eq. (1).

The coupling-constant integration, or switching Hamiltonian method [24], is used to calculate $f(T_0)$. We consider a system with Hamiltonian $H = (1-\lambda)W + \lambda U$, where U describes the actual system (in this work, described with an EAM-type Hamiltonian) and W is the Hamiltonian of the reference system, with known free energy. The parameter λ switches from U (for $\lambda = 1$) to W (for $\lambda = 0$). With this Hamiltonian we can evaluate the free-energy difference between W and U by calculating the reversible work required to switch from one system to the other. The unknown free energy associated with U, $f(T_0)$, is given by

$$\begin{aligned} f^{\mathrm{Sol}}(T_0) &= f_{\mathrm{W}}(T_0) + \Delta f_1,\\ \Delta f_1 &= \frac{1}{N}\int_0^1 \left\langle\frac{\partial H}{\partial\lambda}\right\rangle \mathrm{d}\lambda = \frac{1}{N}\int_0^1 \langle U - W\rangle_\lambda\,\mathrm{d}\lambda, \end{aligned} \tag{2}$$

where $f_{\mathrm{W}}(T_0)$ is the free energy of the reference system at T_0. The integration is carried over the coupling parameter λ that varies between 0 and 1, and $\langle\cdots\rangle$ stands for the average in a (T, V, N) MD simulation.

For the solid phases the reference system W is a set of Einstein oscillators centered on the average atomic positions, in the (T_0, $P = 0$, N) ensemble that is associated with the Hamiltonian U. The free energy per atom of the Einstein crystal that is known analytically [25] is given by

$$f_{\mathrm{Eins}} = -3k_{\mathrm{B}}T_0\ln(T_0/T_{\mathrm{E}}), \tag{3}$$

where T_{E} is the Einstein temperature of the oscillators, $T_{\mathrm{E}} = h\nu_{\mathrm{E}}/k_{\mathrm{B}}$ where k_{B} is the Boltzmann constant, ν_{E} is the frequency of oscillation, and h is the Planck constant. In our calculations we use $T_{\mathrm{E}}^{\mathrm{Cu}} = 343$ K, $T_{\mathrm{E}}^{\mathrm{Fe}} = 470$ K. These values are in fact arbitrary and are chosen so as to make the switching integral, cf. Eq. (2), as smooth as possible to improve numerical accuracy.

For the liquid phase, the reference system W is an ideal gas at the same temperature and density as the EAM sample. The process to switch from U to W involves an intermediate step to avoid particle overlap during the integration, namely we first compute the free-energy difference between the true system with potential U (the EAM potential) and a system with a repulsive potential W_{L} (soft spheres). As in the case of the solid phase, the integration is carried over the coupling parameter λ that varies between 0 and 1. The system is kept at the constant volume V_0, that equilibrates the U Hamiltonian at temperature T_0 and $P = 1$ bar. Therefore, the free-energy change for a pure element due to the switch is given by Δf_1 given by the second line of Eq. (2).

The second step is a reversible expansion of the repulsive gas, from V_0 and high pressure, to the ideal gas limit, where the free energy can be calculated analytically, followed by a reversible compression to recover the initial density. The change in free energy due to both processes is given by

$$\Delta f_2 = k_{\mathrm{B}}T_0\int_0^{\rho_0}\left[\frac{P}{\rho k_{\mathrm{B}}T_0} - 1\right]\frac{\mathrm{d}\rho}{\rho}, \tag{4}$$

where $\rho_0 = N/V_0$ is the particle density. After the processes represented by Eq. (4) have taken place we end up with an ideal gas at (T_0, ρ_0), whose free energy is given analytically by: $f_{\mathrm{W}}^{\mathrm{Liq}}(T_0,\rho_0) = k_{\mathrm{B}}T_0[\ln(\rho_0\Lambda^3) - 1]$, where Λ is the de Broglie thermal wavelength ($\Lambda^2 = h^2/2\pi m k_{\mathrm{B}}T_0$, where m is the atomic mass) [25]. Then the free energy of the liquid phase is calculated as the sum of these 3 contributions,

$$g^{\mathrm{Liq}}(T_0) = \Delta f_1 + \Delta f_2 + f_{\mathrm{W}}^{\mathrm{Liq}}(T_0,\rho_0). \tag{5}$$

Eqs. (1)–(5) give the free energies of the solid and liquid phases for the pure elements as a function of temperature.

The strategy for the alloy follows the same steps as above, and at each composition a random generated sample is used as the starting configuration. For the sample size we use, $(5a_0)^3$, fluctuations of the parameters of interest for different realizations of the random solid solution are of the order of a few meV/atom, which is of the order of the error in the final results, so we use only one sample at each composition. The free energy of the reference mixture of Einstein oscillators can be calculated using the following expression [14]:

$$f_{\mathrm{Eins}}(x,T_0) = x f_{\mathrm{Eins}}^{\mathrm{Cu}} + (1-x)f_{\mathrm{Eins}}^{\mathrm{Fe}} - T_0 s_{\mathrm{conf}}(x), \tag{6}$$

where x measures the Cu composition, and $f^{\mathrm{Cu}}_{\mathrm{Eins}}$ and $f^{\mathrm{Fe}}_{\mathrm{Eins}}$ are given by Eq. (3). The configurational entropy per particle, $s_{\mathrm{conf}}(x)$, is given by the usual expression $-k_{\mathrm{B}}[x\ln\ x+(1-x)\ln(1-x)]$, assuming the solution is completely random. For the ideal gas,

$$f_{\mathrm{id}}(x,T_0,\rho)=xf^{\mathrm{Cu}}_{\mathrm{id}}(\rho_{\mathrm{Cu}})+(1-x)f^{\mathrm{Fe}}_{\mathrm{id}}(\rho_{\mathrm{Fe}}) \tag{7}$$

or, by making the entropy of mixing appear explicitly,

$$f_{\mathrm{id}}(x,T_0,\rho)=xf^{\mathrm{Cu}}_{\mathrm{id}}(\rho)+(1-x)f^{\mathrm{Fe}}_{\mathrm{id}}(\rho)-T_0s_{\mathrm{conf}}(x), \tag{8}$$

where ρ is the total density, ρ_{Cu} and ρ_{Fe} are the partial densities ($x\rho$ and $(1-x)\rho$, respectively), and the f^{i}_{id} are given in the preceding section. These and other useful expressions are carefully worked out in Ref. [14].

These lead to the following general equation for the free energy of each phase Φ:

$$g^{\phi}(x,T)=A^{\phi}(x)+B^{\phi}(x)T+C^{\phi}(x)T^2+D^{\phi}(x)T\ln(T)-Ts_{\mathrm{conf}}(x). \tag{9}$$

Eq. (9) is obtained numerically from computer runs that implement Eqs. (1)–(8) for each phase. We obtain one set of coefficients $\{A,B,C,D\}$ for each composition studied. The relation between these coefficients and the quadratic fit to the enthalpy is $h(T)=a-\mathrm{d}T-cT^2$, while b is given by $b=g(T_0)/T_0-a/T_0-\mathrm{d}\ln T_0-cT_0$.

To match the CALPHAD expression for the Gibbs energy to Eq. (9), this expression is rewritten in terms of three contributions that account for the properties of the pure materials, the linear interpolation between them, and the excess free energy of the mixture, namely:

$$g^{\phi}(x,T)={}^{\mathrm{ref}}g^{\phi}(x,T)+{}^{\mathrm{id}}g^{\phi}_{\mathrm{mix}}(x,T)+{}^{\mathrm{xs}}g^{\phi}_{\mathrm{mix}}(x,T), \tag{10}$$

where the terms on the right-hand side are: the composition-weighted average Gibbs free energy per atom associated with the pure elements (or free energy of the ideal solution), the Gibbs ideal mixing energy, and the excess Gibbs energy due to non-ideal contributions, respectively. The excess Gibbs energy of mixing is expressed by a Redlich–Kister polynomial expansion [26], and then the terms on the right-hand side of Eq. (10), are expressed as follows:

$$\begin{aligned}{}^{\mathrm{ref}}g^{\phi}(x,T)&=(1-x)g^{\phi}_{\mathrm{Fe}}(T)+xg^{\phi}_{\mathrm{Cu}}(T),\\ {}^{\mathrm{id}}g^{\phi}_{\mathrm{mix}}(x,T)&=k_{\mathrm{B}}T[x\ln x+(1-x)\ln(1-x)],\\ {}^{\mathrm{xs}}g^{\phi}_{\mathrm{mix}}(x,T)&=x(1-x)\sum_{p=0}^{n}{}^{p}L^{\phi}(T)(1-2x)^{p},\end{aligned} \tag{11}$$

where ${}^{p}L^{\phi}_{i,j}(T)$ is the pth-order binary interaction parameter relative to phase Φ, that is a function of temperature. Some algebra transforms the set of coefficients in Eq. (9) to those needed in Eq. (11).

Phase stability deserves special consideration in the Fe–Cu system. In nature, as well as in computer simulations, phases usually exist within limited ranges of composition. Based on previous experience with the thermodynamics of EAM Au–Ni alloys [13], and Fe–Cu with the Ackland–Bacon potential [15,16], both solid phases, fcc and bcc, were stable in the simulations at all compositions. With the Fe–Cu Ludwig–Farkas potentials however, the situation is more complex: bcc Cu is unstable and fcc Fe is metastable. This can be seen in Fig. 1 where the energy of both elements at zero temperature is displayed along a Bain distortion. Cu has an energy maximum for the bcc phase, located 46 meV above the fcc energy. Fe in turn has a shallow minimum for the fcc phase, 27 meV above the equilibrium bcc value, but the height of the potential barrier separating both phases is only 31 meV; at room temperature and above, thermal excitations drive Fe away from the fcc phase towards the bcc structure.

However, in numerical simulations on finite systems and short times, this is not always seen, and the instability usually appears as an abnormally large entropy contribution to the free energy as temperature is raised. This translates into an erroneous appearance of these unstable phases in the phase diagram. To solve this problem we have to introduce the stability information as an external

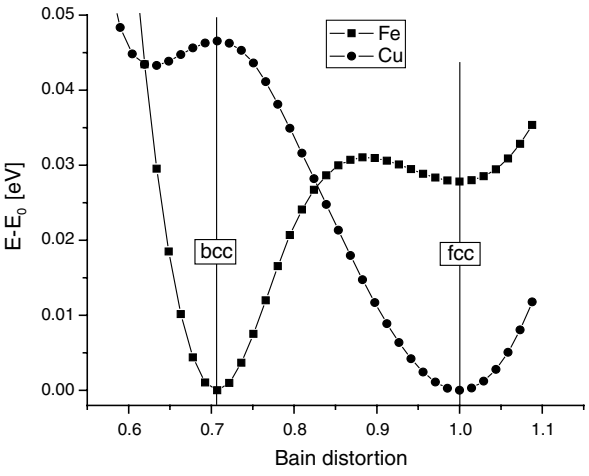

Fig. 1. Energy difference along a Bain distortion with respect to the equilibrium phase for Fe and Cu at 0 K.

constraint, restricting the domain of existence of the phases to the compositions where we know they are definitely stable, namely the bcc-solid solution in the Fe-rich part of the phase diagram, and the fcc-solid solution in the Cu-rich part. We retained then data for Cu compositions up to 20 at.% in bcc, and above 80 at.% in fcc.

Unfortunately, to translate the data into the CALPHAD equations, see Eqs. (10) and (11), that are based on quantities that are in excess with respect to the linear interpolation between the pure elements, we still need expressions for the free energy of fcc Fe and bcc Cu even if they represent unstable or metastable phases. This requirement introduces some arbitrariness in the procedure whose effect is to introduce an uncertainty of ~100 K in the location of the invariant line in the phase diagram. A practical way we have to circumvent this is the following: For unstable bcc Cu we take the free energy corresponding to the stable fcc phase and shift it by the energy of the unstable bcc phase at 0 K, 47 meV/atom (see Fig. 1), namely, $g^{\prime\mathrm{bcc}}_{\mathrm{Cu}}(T) = g^{\mathrm{fcc}}_{\mathrm{Cu}}(T) + \Delta E^{\mathrm{bcc-fcc}}_{\mathrm{Cu}}(T = 0\ \mathrm{K})$. For the free energy of the fcc phase of Fe we use the value obtained even if it is affected by finite size effects, and shift it by +15 meV/atom to avoid the intrusion of this phase in the Fe-rich part of the diagram, namely $g^{\prime\mathrm{fcc}}_{\mathrm{Fe}}(T) = g^{\mathrm{fcc}}_{\mathrm{Fe}}(T) + 15\,\mathrm{meV/atom}$. We explored several other alternatives, but none seems better justified; 15 meV/atom is the minimum shift value that avoids the appearance of the fcc phase in the Fe-rich region of the phase diagram. The need of anchoring points at $x = 0$ and $x = 1$ forces us to define energies of non-existing (unstable) phases for which, strictly speaking, the Gibbs energies are ill defined. This difficulty is inherent to the CALPHAD formalism and is also encountered when dealing with experimental data requiring anchoring points on phases that are not experimentally accessible. Fig. 2(a)–(d) show the location of these points in the four coefficients entering the definition of g, Eq. (9): Solid squares represent data for the fcc phase, with values for $0.8 < x_{\mathrm{Cu}} < 1.0$ and anchoring point at $x_{\mathrm{Cu}} = 0.0$; open squares represent data for the bcc phase between $0.0 < x_{\mathrm{Cu}} < 0.2$, with anchoring point at $x_{\mathrm{Cu}} = 1.0$. With these considerations, the coefficients appearing in Eq. (9) for the three phases (ϕ = liquid, fcc, bcc), as obtained from our numerical simulations, are reported in Tables 1–3. From the structure of these data we choose to

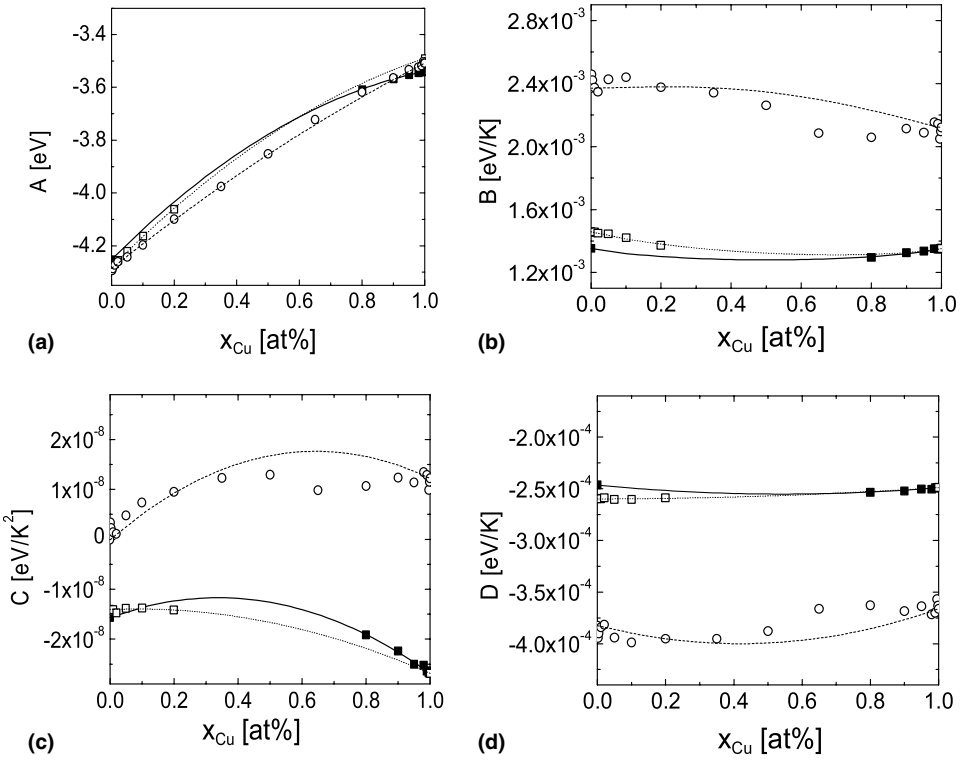

Fig. 2. Coefficients A, B, C, and D of the free energy, Eq. (9), for each phase: liquid (open circles), fcc (solid squares), bcc (open squares).

Table 1
Coefficients of the free energy as a function of temperature, cf. Eq. (9), for the fcc phase of Fe–Cu alloys

x_{Cu}^{fcc}	A [eV]	B [eV/K]	C [eV/K^2]	D [eV/K]
0	−4.25138	1.45938E−03	−1.40062E−08	−2.59855E−04
0.8	−3.60832	1.29580E−03	−1.91789E−08	−2.53386E−04
0.9	−3.56729	1.32543E−03	−2.23772E−08	−2.52135E−04
0.95	−3.55086	1.33524E−03	−2.50435E−08	−2.50261E−04
0.98	−3.54342	1.35094E−03	−2.51903E−08	−2.50525E−04
0.99	−3.54145	1.34823E−03	−2.64303E−08	−2.49216E−04
0.996	−3.54026	1.34867E−03	−2.67759E−08	−2.48917E−04
0.998	−3.53997	1.35420E−03	−2.64241E−08	−2.49379E−04
1	−3.53953	1.35140E−03	−2.68433E−08	−2.48949E−04

Table 2
Coefficients of the free energy as a function of temperature, cf. Eq. (9), for the bcc phase of Fe–Cu alloys

x_{Cu}^{bcc}	A [eV]	B [eV/K]	C [eV/K^2]	D [eV/K]
0	−4.28000	1.45938E−03	−1.40062E−08	−2.59855E−04
0.001458	−4.27806	1.45599E−03	−1.42382E−08	−2.59431E−04
0.004373	−4.27443	1.45423E−03	−1.43561E−08	−2.59279E−04
0.010204	−4.26762	1.45695E−03	−1.41322E−08	−2.59716E−04
0.020408	−4.25453	1.44906E−03	−1.47284E−08	−2.58906E−04
0.049563	−4.22048	1.44485E−03	−1.38446E−08	−2.60285E−04
0.100583	−4.16233	1.42072E−03	−1.37780E−08	−2.60295E−04
0.199708	−4.06114	1.37250E−03	−1.41451E−08	−2.58918E−04
1	−3.49	1.35140E−03	−2.68433E−08	−2.48949E−04

Table 3
Coefficients of the free energy as a function of temperature, cf. Eq. (9), for the liquid phase of Fe–Cu alloys

x_{Cu}^{Liq}	A [eV]	B [eV/K]	C [eV/K^2]	D [eV/K]
0	−4.28610	2.37097E−03	−6.76295E−11	−3.82451E−04
0.002	−4.29362	2.45791E−03	3.31948E−09	−3.94422E−04
0.004	−4.28674	2.42227E−03	2.23661E−09	−3.89912E−04
0.01	−4.27355	2.37365E−03	1.42533E−09	−3.84300E−04
0.02	−4.26018	2.34670E−03	1.13394E−09	−3.81570E−04
0.05	−4.24251	2.42697E−03	4.76908E−09	−3.94123E−04
0.1	−4.19793	2.43993E−03	7.35201E−09	−3.98762E−04
0.2	−4.10003	2.37639E−03	9.49156E−09	−3.95188E−04
0.35	−3.97537	2.34051E−03	1.22849E−08	−3.95192E−04
0.5	−3.85195	2.26136E−03	1.29294E−08	−3.87798E−04
0.65	−3.72193	2.08482E−03	9.86382E−09	−3.66247E−04
0.8	−3.61760	2.05798E−03	1.06525E−08	−3.62702E−04
0.9	−3.56444	2.11319E−03	1.23469E−08	−3.68471E−04
0.95	−3.53277	2.08774E−03	1.14054E−08	−3.63898E−04
0.98	−3.52391	2.15427E−03	1.34532E−08	−3.71691E−04
0.99	−3.51786	2.14454E−03	1.28951E−08	−3.69887E−04
0.996	−3.50209	2.04871E−03	9.90364E−09	−3.56993E−04
0.998	−3.50700	2.09668E−03	1.15027E−08	−3.63299E−04
1	−3.50855	2.12037E−03	1.22168E−08	−3.66211E−04

attempt a quadratic fit to determine the coefficients ${}^0L^{\phi}(T)$ appearing in Eq. (11). This is equivalent to choosing to describe this alloy with only the L-term with $p = 0$ in the polynomial expression (9), namely:

$$i^{\phi} = x(1-x)^0 L_i^{\phi} + x i_{Cu}^{\phi} + (1-x) i_{Fe}^{\phi}, \tag{12}$$

where i stands for A, B, C, and D. The ${}^0L^{\phi}(T)$ are determined from these fits as:

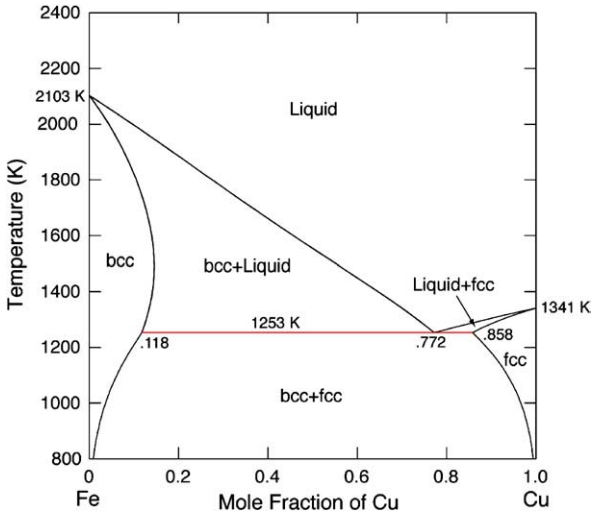

Fig. 3. Phase diagram corresponding to the Ludwig–Farkas EAM potentials for Fe–Cu alloys.

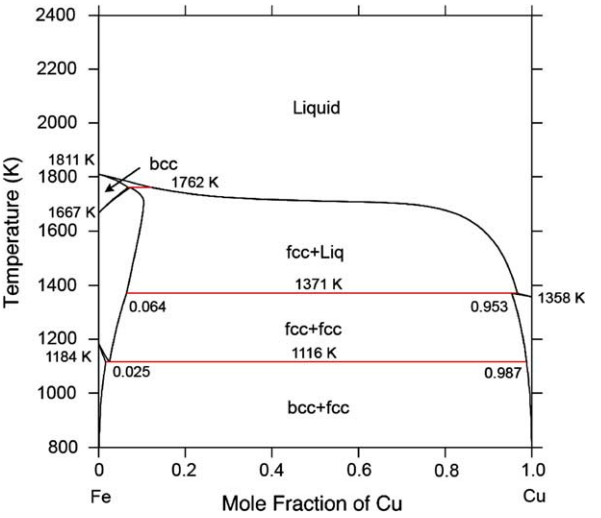

Fig. 4. Fe–Cu phase diagram obtained from CALPHAD data.

$$^{0}L^{\phi}(T) = {}^{0}L^{\phi}_{a} + {}^{0}L^{\phi}_{b}T + {}^{0}L^{\phi}_{c}T^{2} + {}^{0}L^{\phi}_{d}T\ln(T). \qquad (13)$$

With these quantities we have all the information needed to calculate the phase diagram. Appendix I contains the numerical expressions that can be used 'manually' with the common tangent construction, or be input into Thermo-Calc [22] to automatically obtain phase diagram information. Fig. 3 shows the Fe–Cu phase diagram corresponding to the Ludwig–Farkas EAM potentials.

3. Discussion

Comparison between the phase diagram displayed in Fig. 3 and the experimental one [27] depicted in Fig. 4, shows reasonable topological agreement up to 1000 K. At higher temperatures noticeable differences appear. The origin of these discrepancies can be analyzed by examining the high-temperature properties of the pure elements, and those of the (fcc and bcc) solid solutions.

With the EAM potential of Ref. [17], Cu exhibits a fcc phase that melts at 1341 K, a temperature quite close to the experimental value of 1358 K. In Fig. 5 (left panels) the results for the enthalpy, entropy and Gibbs free energy for this potential as functions of temperature are compared with those from the solid solution database (SSOL) from Thermo-Calc [22]. The agreement between the two sets of results is quite satisfactory at least below 2000 K. The bcc phase of Cu with this EAM potential is found unstable, as confirmed by its elastic constants calculated at 0 K: $C_{11} = 0.952\ \text{eV/Å}^3$ and $C_{12} = 1.012\ \text{eV/Å}^3$, with $C' = 1/2(C_{11} - C_{12})$ being negative. It is worth noting that according to the CALPHAD database, the bcc phase is stable, although it does not explicitly affect the phase diagram. Thus the instability introduces suspicions about the ability of this potential to describe Cu precipitates that, when small in size, are known to be bcc. The evolution with size of a cluster of Cu precipitates will not only be affected by the effects of the constraint from the surrounding solvent, but also by the relative stability of the bcc Cu phase. Moreover it seems to have been unnoticed when the Fe and Fe–Cu potentials were published [10,17]. For precipitation studies, the necessity of having a bcc phase with the right energetics as a function of temperature can not be overstated since any study of precipitation will be affected by it.

Contrary to the potentials studied here, in our previous study on the Ackland–Bacon EAM Fe–Cu potentials [15,16], we reported a bcc phase of Cu so stable that it entered the equilibrium phase diagram. As said before, the free energy of bcc Cu is reported in the CALPHAD database. However, in the empirical potentials developed so far, the properties of the bcc phase come out with little or no control from the potential developers. As a conclusion we observe that despite the fact that Cu is the element best described with EAM, further attempts to reproduce the right thermodynamics of its bcc phase may help to improve the capabilities of the potential. Such attempts are currently undertaken, and improved potentials for Cu are becoming

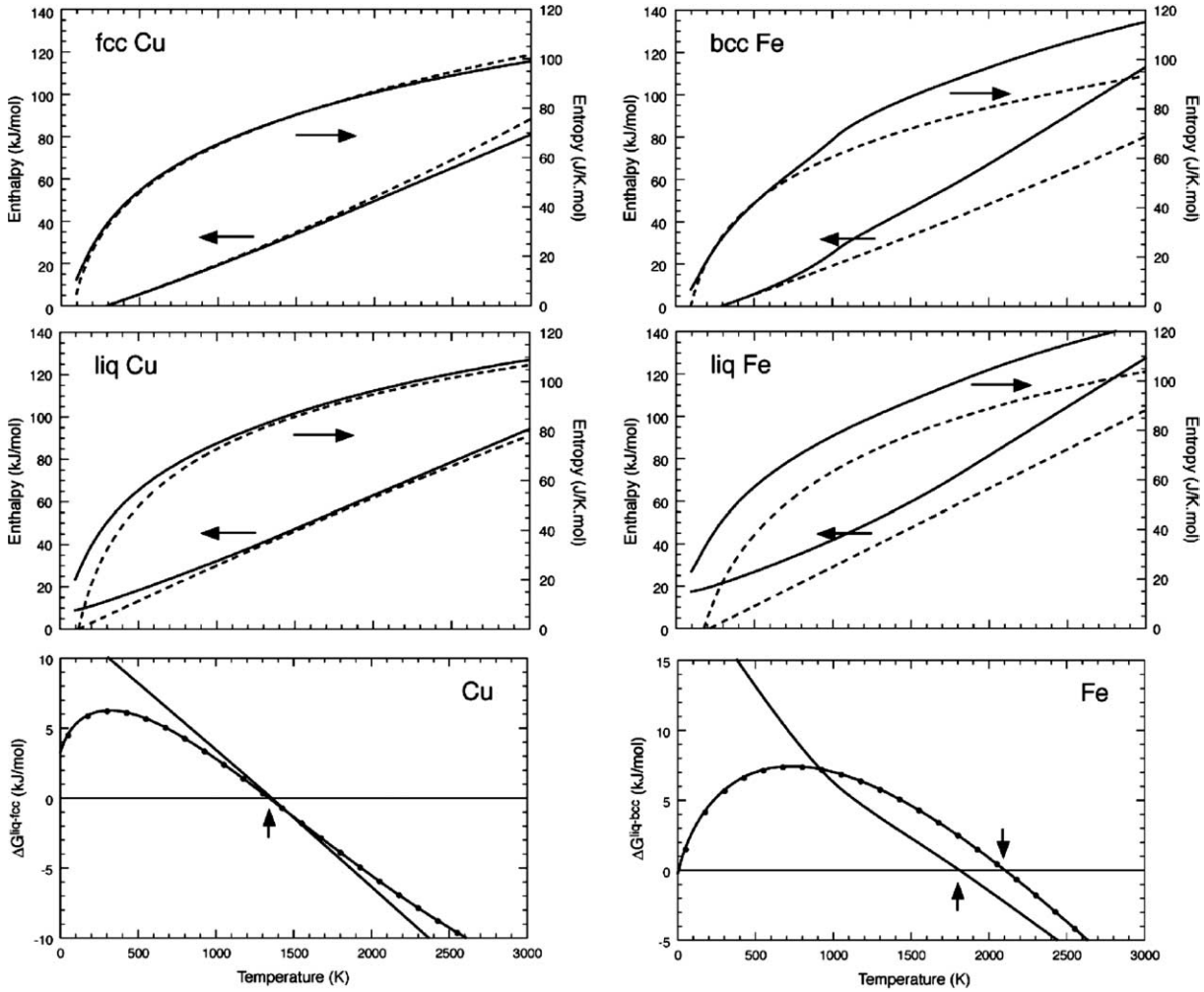

Fig. 5. Enthalpy (in kJ/mol) and entropy (in J/K mol) as functions of temperature for the fcc (bcc), and liquid phases of pure Cu (Fe) in the left (right) panel. The bottom figures show the structural molar Gibbs energy differences (in kJ/mol) liq-fcc for Cu (left) and liq-bcc for Fe (right), and the arrows indicate the location of the melting points. The solid lines refer to the CALPHAD results obtained from the SSOL database whereas the dashed and dotted solid lines correspond to the EAM-derived results.

available such as the one developed by Mishin et al. [28] for diffusion studies.

With the EAM potential of Ref. [18], pure Fe shows a bcc phase stable until melting occurs at a temperature 28% higher than the experimental value. The fcc phase of Fe is unstable above room temperature. This fact is confirmed by the values of the elastic constants calculated at 0 K. For fcc Fe in Ref. [18], $C_{11} = 0.998\ \text{eV/Å}^3$ and $C_{12} = 0.808\ \text{eV/Å}^3$, and therefore $C' = 0.190\ \text{eV/Å}^3$, a suspiciously small value that presumably goes negative at some finite temperature. None of the potentials available so far for Fe predict the existence of the fcc phase at high temperatures, as expected, because it is the result of a fundamental change in its electronic structure and magnetic properties rather than in a mere competition between enthalpy and entropy as T varies. However, Fe melts in the bcc phase, and therefore it would be possible to significantly improve the melting point by adjusting the properties of the bcc and the liquid phases. In Fig. 5 (right panels) the results obtained with the present EAM potential for the enthalpy, entropy and Gibbs free energy are compared with those derived from the SSOL database as functions of temperature. As in the case of the Ackland–Bacon EAM potential [15,16], the discrepancies are severe for the enthalpy and the entropy at high temperature above 1000 K for reasons mentioned above although the melting point has been improved

(2103 K compared with 2381 K for the Ackland–Bacon EAM potential and 1811 K for the experimental value). Despite the large effort undertaken to develop improved Fe potentials, such as the one recently reported by Ackland et al. [29], no thermodynamic analysis has been reported yet to judge the quality of the potential.

The Fe–Cu alloy shows an eutectic at $x_{Cu} = 0.75$. In the experimental/CALPHAD phase diagram a peritectic appears because the liquidus in the Cu-rich region is located at higher temperature than melting of pure Cu and the peritectic reaction is $L + Fe_{fcc} \rightarrow Cu_{fcc}$. In our case, the potential would hardly predict the peritectic point in the Cu rich portion of the phase diagram, given that the fcc Fe phase never appears. Solubility limits are in reasonable agreement with experimental values. The almost symmetric behavior of these limits is consistent with the retention of only the $p = 0$ term in the Redlich–Kister expansion for the excess Gibbs energy, Eq. (11), and with the experimental data as well.

The behavior of these potentials for the Fe–Cu mixture was modeled on the basis of the dilute limits of the heats of solution, and this is to our knowledge the strategy consistently followed for all alloys described so far in the literature within the EAM framework. The mixed pair potential is the only function that contains information about the alloying effects. It can easily be shown that there is a one to one relation between this formulation and the fact that the excess enthalpy of mixing at 0 K is a single-parameter quadratic curve, i.e., a curve that only needs the term $p = 0$ in the Redlich–Kister expansion. Besides the more involved contributions coming from entropy, we can analyze the adequacy of this symmetric single parameter description of excess enthalpy of mixing by looking at its contribution at 0 K and comparing it with the CALPHAD database. Fig. 6 shows the SSOL values and those from this potential, for both bcc and fcc phases. The agreement is remarkably good. Within a few percent, EAM and CALPHAD values compare favorably, and even more so in the regions of interest, i.e., $x \ll 1$ for bcc and $x \sim 1$ for fcc solid solutions. Despite the excellent agreement it can be noted that the location of the *solvus* line in bcc Fe appears to be shifted to larger Cu compositions relative to the experimental/CALPHAD phase diagram indicating the significant effect of entropy. Note that the agreement for the liquid phase is rather poor.

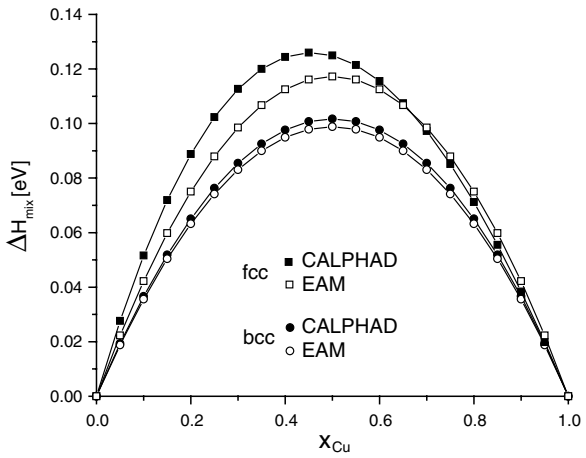

Fig. 6. Excess enthalpy of mixing at 0 K for both fcc and bcc Fe–Cu solid solutions. Open symbols: EAM results, solid symbols CALPHAD data.

With these observations we conclude by highlighting the fact that alloy description is essentially composed of two distinct contributions. One is the description of the pure elements that, in the case under study, is not very satisfactory at high temperatures. The other is the description of the mixture that, for this alloy, is remarkably accurate up to 1000 K. The necessity of a more accurate description of mixtures at high temperatures is evident, as in general, the $p = 0$ approximation in Eq. (11) is not sufficient to describe most systems of interest. Our analysis indicates that the EAM potentials discussed here can be used up to 1000 K, and that for higher temperatures, improved potentials primarily for the pure components should be developed to account for proper phase stability in the solid phase up to melting.

Regarding this last comment, we have recently published a method to describe arbitrarily complex formation energies via a generalization of the EAM that includes concentration dependent interactions [30]. These interactions are defined in such a way that the formation enthalpy of the alloy under consideration is fitted. We applied the method to Fe–Cr alloys, where recent ab initio results predict a complex behavior of the 0 K formation energy [31], and arrived at a potential which is able to reproduce the order tendencies reported for this alloy.

Acknowledgments

Discussions with Larry Kaufman are gratefully acknowledged. Work performed under the auspices

of the US Department of Energy by the University of California Lawrence Livermore National Laboratory under contract No. W-7405-ENG-48, and CONICET, Argentina, PIP-0664/98.

Appendix I

Free energies for all phases of pure elements and coefficient for the Redlich–Kister expansions of the excess free energy of mixing, Eq. (11), for Fe–Cu alloys

$$g_{\mathrm{Fe}}^{\mathrm{fcc}} = -4.25138054 - 2.4630144 \times 10^{-4} T \ln(T) - 1.5632073 \times 10^{-8} T^2 + 1.3533511 \times 10^{-3} T,$$

$$g_{\mathrm{Fe}}^{\mathrm{bcc}} = -4.27999730 - 2.5985509 \times 10^{-4} T \ln(T) - 1.4006218 \times 10^{-8} T^2 + 1.4593817 \times 10^{-3} T,$$

$$g_{\mathrm{Fe}}^{\mathrm{Liq}} = -4.28610001 - 3.8245119 \times 10^{-4} T \ln(T) - 6.7629536 \times 10^{-11} T^2 + 2.3709670 \times 10^{-3} T,$$

$$g_{\mathrm{Cu}}^{\mathrm{fcc}} = -3.53953201 - 2.4894946 \times 10^{-4} T \ln(T) - 2.6843291 \times 10^{-8} T^2 + 1.3514004 \times 10^{-3} T,$$

$$g_{\mathrm{Cu}}^{\mathrm{bcc}} = -3.49000 - 2.4894946 \times 10^{-4} T \ln(T) - 2.6843291 \times 10^{-8} T^2 + 1.3514004 \times 10^{-3} T,$$

$$g_{\mathrm{Cu}}^{\mathrm{Liq}} = -3.50855397 - 3.6621148 \times 10^{-4} T \ln(T) + 1.2216831 \times 10^{-8} T^2 + 2.1203670 \times 10^{-3} T,$$

$${}^{0}L^{\mathrm{fcc}} = 0.46899 - 5.0 \times 10^{-5} T + 3.4541 \times 10^{-8} T^2 - 3 \times 10^{-5} T \ln(T),$$

$${}^{0}L^{\mathrm{bcc}} = 0.39539 - 9.0 \times 10^{-5} T + 1.5131 \times 10^{-8} T^2 - 1 \times 10^{-5} T \ln(T),$$

$${}^{0}L^{\mathrm{Liq}} = 0.17057 + 6.4 \times 10^{-4} T + 4.2784 \times 10^{-8} T^2 - 1 \times 10^{-4} T \ln(T).$$

References

[1] W.J. Phythian, A.J.E. Foreman, C.A. English, J.T. Buswell, M.G. Hetherington, K. Roberts, S. Pizzini, in: 15th International Symposium on 'Effects of Radiation on Materials', Nashville, Tennessee, 19–21 June 1990ASTM STP, 1125, American Society for Testing and Materials, Philadelphia, 1992, p. 131.
[2] W.J. Phythian, C.A. English, J. Nucl. Mater. 205 (1993) 162.
[3] G.J. Ackland, D.J. Bacon, A.F. Calder, T. Harry, Philos. Mag. A 75 (1997) 713;
See also G.J. Ackland, G. Tichy, V. Vitek, M. Finnis, Philos. Mag. A 56 (1987) 735.
[4] Yu.N. Osetsky, A.G. Mikhin, A. Serra, Philos. Mag. A 72 (1995) 361.
[5] Yu.N. Osetsky, A. Serra, Philos. Mag. A 73 (1996) 249.
[6] Yu.N. Osetsky, A. Serra, Philos. Mag. A 75 (1997) 1097.
[7] G.R. Odette, B.D. Wirth, J. Nucl. Mater. 251 (1997) 157.
[8] B.D. Wirth, G.R. Odette, Mater. Res. Soc. Symp. Proc. 540 (1999) 637.
[9] C. Domain, C.S. Becquart, J.C. Van Duysen, Mater. Res. Soc. Symp. Proc. 540 (1999) 643.
[10] M. Ludwig, D. Farkas, D. Pedraza, S. Schmauder, Model. Simul. Mater. Sci. Eng. 6 (1998) 19.
[11] Y. Le Bouar, Acta Mater. 49 (2001) 2661.
[12] J.J. Blackstock, G.J. Ackland, Philos. Mag. A 81 (2001) 2127.
[13] E.O. Arregui, M. Caro, A. Caro, Phys. Rev. B 66 (2002) 054201.
[14] E.O. Arregui, M. Caro, A. Caro, Comput. Mater. Sci. 25 (2002) 297.
[15] E.M. Lopasso, M. Caro, A. Caro, P.E.A. Turchi, Phys. Rev. B 68 (2003) 214205.
[16] A. Caro, P.E.A. Turchi, M. Caro, E.M. Lopasso, J. Nucl. Mater. 336 (2005) 233.
[17] A.F. Voter, Los Alamos Unclassified Technical Report 93-3901, Los Alamos National Laboratory.
[18] G. Simonelli, R. Passianot, E.J. Savino, Mater. Res. Soc. Proc. 291 (1993) 567.
[19] L. Kaufman, H. Bernstein, Computer Calculation of Phase Diagrams with Special Reference to Refractory Metals, Academic Press, New York, 1970.
[20] N. Saunders, A.P. Miodownik, CALPHAD, Calculation of Phase Diagrams: A Comprehensive Guide, Pergamon Materials Series, vol. 1, Pergamon, 1998.
[21] I. Ansara, B. Sundman, in: P.S. Glaeser (Ed.), The Scientific Group Thermodata Europe, Computer Handling and Dissemination of Data, Elsevier Science Pub. Co., 1987.
[22] B. Sundman, B. Jansson, J.-O. Andersson, CALPHAD 9 (1985) 153;
P.J. Spencer (guest ed.), Computer Simulations from Thermodynamic Data: Materials Production and Development, MRS Bulletin, vol. 24 (4), Materials Research Society, Warrendale, PA, April 1999, p. 18.
[23] A. Dinsdale, CALPHAD 15 (1991) 317.
[24] G. Ciccotti, W.G. Hoover (Eds.), Molecular-Dynamics Simulation of Statistical-Mechanical Systems, North-Holland, Amsterdam, 1986.
[25] D. Frenkel, B. Smit, Understanding Molecular Simulation—From Algorithms to Applications, Academic Press, London, 1996.
[26] O. Redlich, A. Kister, Ind. Eng. Chem. 40 (1948) 345.
[27] T.B. Massalski (Ed.), Binary Alloy Phase Diagrams, second ed., ASM International, Metals Park, OH, 1990.
[28] Y. Mishin, M.J. Mehl, D.A. Papaconstantopoulos, A.F. Voter, J.D. Kress, Phys. Rev. B 63 (22) (2001) 224106.
[29] G.J. Ackland, M.I. Mendelev, D.J. Srolovitz, S. Han, A.V. Barashev, J. Phys.: Condens. Matter 16 (27) (2004) S2629.
[30] A. Caro, D. Crowson, M. Caro, Phys. Rev. Lett. 95 (2005) 075702.
[31] P. Olsson, I.A. Abrikosov, L. Vitos, J. Wallenius Jr., Nucl. Mater. 321 (2003) 84.